Biosensors and Bioelectronics 26 (2010) 390–397

Contents lists available at ScienceDirect

Biosensors and Bioelectronics

journal homepage: www.elsevier.com/locate/bios

Direct electrochemistry and electrocatalysis of novel single-walled carbon nanotubes–hemoglobin composite microbelts—Towards the development of sensitive and mediator-free biosensor

Yu Ding, Ying Wang, Yu Lei*

Department of Chemical, Materials and Biomolecular Engineering, University of Connecticut, 191 Auditorium Road, Storrs, CT 06269, USA

ARTICLE INFO

Article history:
Received 14 May 2010
Received in revised form 9 July 2010
Accepted 30 July 2010
Available online 12 August 2010

Keywords:
Hemoglobin
Electrospinning
Microbelts
Single-walled carbon nanotubes
Biosensor

ABSTRACT

Single-walled carbon nanotubes (SWNTs) and hemoglobin (Hb) were co-electrospun to generate SWNTs–Hb microbelts, a novel composite material combining the advantages of excellent electron transfer property of SWNTs, electrocatalytic capability of redox Hb proteins, and highly porous structure of microbelts. FT-IR spectra confirmed that Hb in the microbelts kept its native conformational structure and Raman spectra demonstrated the successful incorporation of SWNTs in the microbelts. The direct electrochemistry of SWNTs–Hb composite microbelts was investigated and its application for electrocatalytic reductions and sensitive detections of three compounds, trichloroacetic acid (TCA), nitrite, and hydrogen peroxide (H_2O_2) was also conducted. The SWNTs–Hb composite microbelts based amperometric biosensor showed fast responses to the analytes with excellent detection limits of 2.41 μM for TCA, 0.30 μM for nitrite, and 0.22 μM for H_2O_2 (S/N = 3), and superior apparent Michaelis–Menten constants of 0.24, 0.491 and 0.070 mM for TCA, nitrite and H_2O_2, respectively. Its application for spiked tap water was also demonstrated. The comparison of the SWNTs–Hb composite microbelts modified electrode with other reported electrodes in the literature indicates that the incorporation of SWNTs into Hb microbelts can significantly enhance the direct electrochemistry of Hb and the SWNTs–Hb microbelts based biosensor has great potential application in the mediator-free detection of various analytes.

Published by Elsevier B.V.

1. Introduction

Hemoglobin (Hb), a well-known oxygen-carrying redox protein, is a tetrameric protein consisting of four subunits and each subunit is a combination of a polypeptide chain and a heme group. The heme group consists of an iron atom (Fe^{2+} or Fe^{3+}) attached to a planar organic structure belonging to porphyrin compounds and endows the brown color to the protein. Owing to its known and documented structure, commercial availability and moderate cost, Hb has been extensively used as an ideal model molecule for the study of direct electron transfer process and in the construction of biosensors (He and Zhu, 2006). Generally, the direct electron transfer between Hb and conventional electrodes is slow due to the deep burying of electroactive prosthetic groups as well as unfavorable orientation and/or adsorptive denaturation of Hb on the electrode surface (Han et al., 2002), thus greatly limiting the performance of Hb-based biosensors. Therefore, to facilitate the direct electron transfer between Hb and electrode is of great importance in the development of Hb-based biosensors, but is also very challenging.

With the development of nanotechnology, various nanoparticles such as Au (Maduralveeran and Ramaraj, 2007), Ag (Zhao et al., 2006), quantum dots (Cai et al., 2008), $CaCO_3$ (Shan et al., 2007), and clay (Liu et al., 2005), and nanotubes such as TiO_2 nanotubes (Gao et al., 2008), silica nanotubes (Kapoor et al., 2009), and carbon nanotubes (Cai and Chen, 2004a) have been exploited to accelerate electron transfer between Hb and electrodes. Among all these nanomaterials, carbon nanotubes (CNTs) have been attracting more and more attentions owing to their good electronic properties, superior mechanical strength, and biocompatibility. The utilization of CNTs in the electrochemical study of redox protein can offer effective electron-conducting tunnels, reduce the insulating property of proteins, and thus facilitate direct electron transfer between electrode and redox proteins (Sun et al., 2009a). However, a matrix film is usually required to entrap CNTs and Hb, and thus immobilize them on the electrode surface. A variety of materials have been employed as the matrix, including Nafion (Cai and Chen, 2004a), sodium alginate (SA) (Zhao et al., 2009), polyvinyl alcohol (PVA) (Sun et al., 2009a), and chitosan (Chen et al., 2008). These entrapment materials, to a certain extent, lead to an additional diffusion resistance and reduce the affinity of proteins to the analyte, and hence sacrifice the sensitivity, the detection limit, and biocompatibility. Especially for Nafion, it is anionic and can exclude negatively

* Corresponding author. Tel.: +1 860 486 4554; fax: +1 860 486 2959.
E-mail address: ylei@engr.uconn.edu (Y. Lei).

0956-5663/$ – see front matter Published by Elsevier B.V.
doi:10.1016/j.bios.2010.07.124

charged analytes such as nitrite, compromising the sensitivity and the limit of detection (Njagi et al., 2010). Another drawback of the entrapment method lies in the possible leakage of Hb and CNTs into the electrolyte, thus reducing the stability of biosensor.

In this study, Hb and single-walled carbon nanotubes (SWNTs) were dissolved/suspended in 2,2,2-trifluoroethanol (TFE) and the mixture was directly electrospun onto the surface of glassy carbon electrode (GCE) to fabricate SWNTs–Hb composite microbelts modified GCE (denoted as SWNTs–Hb microbelts/GCE). To the best of our knowledge, this is the first time that SWNTs are incorporated into protein microbelts through electrospinning process and utilized to construct SWNTs–Hb microbelts based mediator-free biosensor. Scanning electron microscope (SEM), FT-IR and Raman spectra were employed to characterize the as-electrospun SWNTs–Hb microbelts. Cyclic voltamogramms (CVs) were conducted to study the direct electrochemistry of the SWNTs–Hb composite microbelts and their electrocatalytic reduction properties for trichloroacetic acid (TCA), nitrite, and hydrogen peroxide (H_2O_2). Sensitive amperometric detection of these three analytes was also demonstrated. TCA, nitrite and H_2O_2 were chosen as the targets due to following reasons. TCA is produced from chlorination during the treatment of drinking water as a disinfection byproduct which has potentially mutagenic and carcinogenic effects on animals and human (Suedee et al., 2007). Nitrite has been widely used in the environment, beverage and food products as a preservative owing to the anti-microbial action of nitrite. However, nitrite has carcinogenic effects and can be toxic in high concentration to animals. H_2O_2 is a product of enzymatic reactions catalyzed by a large number of oxidases (e.g. glucose oxidase and peroxidase) and thus is practically important in the field of biosensor development. Based on the amperometric response, the corresponding calibration curves and apparent Michaelis–Menten constants were also obtained. The results indicate that the incorporation of SWNTs in Hb microbelts can greatly enhance the performance of Hb and the novel SWNTs–Hb composite microbelts are promising in the development of sensitive and mediator-free biosensors.

2. Experimental

2.1. Reagents

Bovine Hb (64.5 kDa) was obtained from MP Biomedicals. TFE, 30 wt% H_2O_2, and TCA were purchased from Fisher Scientific. SWNTs (purity > 90 wt%, outer diameter of 1–2 nm, length of 5–30 μm) were bought from Cheap Tubes Inc. (Vermont, USA). All reagents were used without further treatment. 0.1 M phosphate buffer solutions with various pH values and 0.05 M pH 4.0 Britton–Robinson (BR) buffer were used as supporting electrolytes in the electrochemical experiments. All aqueous solutions were prepared using deionized water (18.2 MΩ cm).

2.2. Fabrication of the SWNTs–Hb microbelts modified GCE

SWNTs were ultrasonicated in TFE for 6 h to obtain homogenous suspension and then Hb was dissolved in the suspension. The final concentration of Hb was 175 mg/mL while the concentration of SWNTs was varied (0, 5, and 10 mg/mL). Electrospinning was carried out using a 19 gauge needle with a flow rate of 1.8 mL/h at an applied potential of 22.5 kV over a collection distance of 12 cm.

GCE (diameter 3 mm) was polished with 1 and 0.05 μm slurries sequentially, and then rinsed with DI water thoroughly. After that, the electrode was sonicated in ethanol and then in DI water, followed by drying at room temperature. SWNTs–Hb microbelts were directly electrospun onto the surface of GCE. After the electrospinning, the GCE modified with electrospun SWNTs–Hb microbelts was then placed in glutaraldehyde (GA) vapor for crosslinking, resulting water-insoluble SWNTs–Hb microbelts. Before the use of modified GCE, it was immersed in pH 7.0 phosphate buffer (0.1 M) at 4 °C for at least 2 h to wet SWNTs–Hb microbelts thoroughly.

2.3. Apparatus and electrochemical measurements

FT-IR spectra were obtained on a Nicolet Magna-IR 560 spectrophotometer (Bruker, Germany). Raman spectra were recorded at ambient temperature on a Renishaw Ramanscope Micro-Raman with 514 nm wavelength laser. Cyclic voltammetry (CV) measurements were performed on a Model CHI 601C electrochemical workstation (CH Instruments, USA). All experiments were conducted using a three-electrode electrochemical cell. The modified electrodes or bare GCE were used as working electrodes, a platinum wire electrode and an Ag/AgCl, 3 M KCl electrode as auxiliary and reference electrode, respectively. Prior to the electrochemical measurements, the solutions were purged with high-purity nitrogen for 20 min and a nitrogen atmosphere was kept over the solution during measurements to eliminate the interference from oxygen reduction. For amperometric detection, all measurements were performed by applying an appropriate potential to the working electrode and allowing the transient background current to decay to a steady-state value, before the addition of the analyte (TCA, NO_2^- or H_2O_2). A stirred solution was employed to provide convective transport in amperometric detection.

3. Results and discussion

3.1. Characterization of SWNTs–Hb microbelts

Fig. 1a–c shows the optical images of electrospun SWNTs–Hb microbelts with different ratios of SWNT to Hb (0/175, 5/175, and 10/175 mg/mg). The corresponding SEM images are presented in Fig. 1d–f. Without SWNTs, Hb microbelts display the typical brown color due to the presence of heme groups. However, with the increase of the ratio of SWNT to Hb in microbelts from 0/175 to 10/175, the color of microbelts changes to black, indicating that SWNTs have been incorporated into the microbelts. In addition, the SEM images show that the Hb microbelts have an average width of ~2.5 μm and the thickness of ~600 nm, however, the width and thickness of microbelts slightly increases with the increase of the ratio of SWNT to Hb, meanwhile the distribution of the microbelts becomes broader in terms of the width of microbelts. The effect of SWNTs concentration on the width and thickness microbelts was presented in Fig. S1. When the ratio of SWNT to Hb goes up to 15 mg SWNT/175 mg Hb, the microbelts can hardly be formed due to the extremely high viscosity of the mixture. As the higher content of SWNTs in the microbelts results in better electrochemical signal in the electrochemical studies (data not shown), the SWNTs–Hb microbelts prepared from a mixture containing 10 mg/mL SWNTs and 175 mg/mL Hb were used for subsequent experiments.

The conformational integrity of Hb in the as-electrospun composite microbelts is critical in the subsequent study of its direct electrochemistry and electrocatalytic properties. Therefore, FT-IR spectra of native Hb powder (curve a), the Hb microbelts (curve b), the SWNTs–Hb microbelts (curve c), and SWNTs powder (curve d) were investigated and presented in Fig. S2A. The amide I band at 1650 cm^{-1} results from C=O stretching vibrations of the peptide linkage while the amide II band at 1535 cm^{-1} is caused by a combination of N–H in-plane blending and C–N stretching of the peptide groups (Zhao et al., 2009). It can be seen that FT-IR spectra for Hb microbelts and SWNT-Hb microbelts show similar amide I and II bands as those observed in the spectrum of native Hb powder, indicating that Hb in SWNTs–Hb microbelts

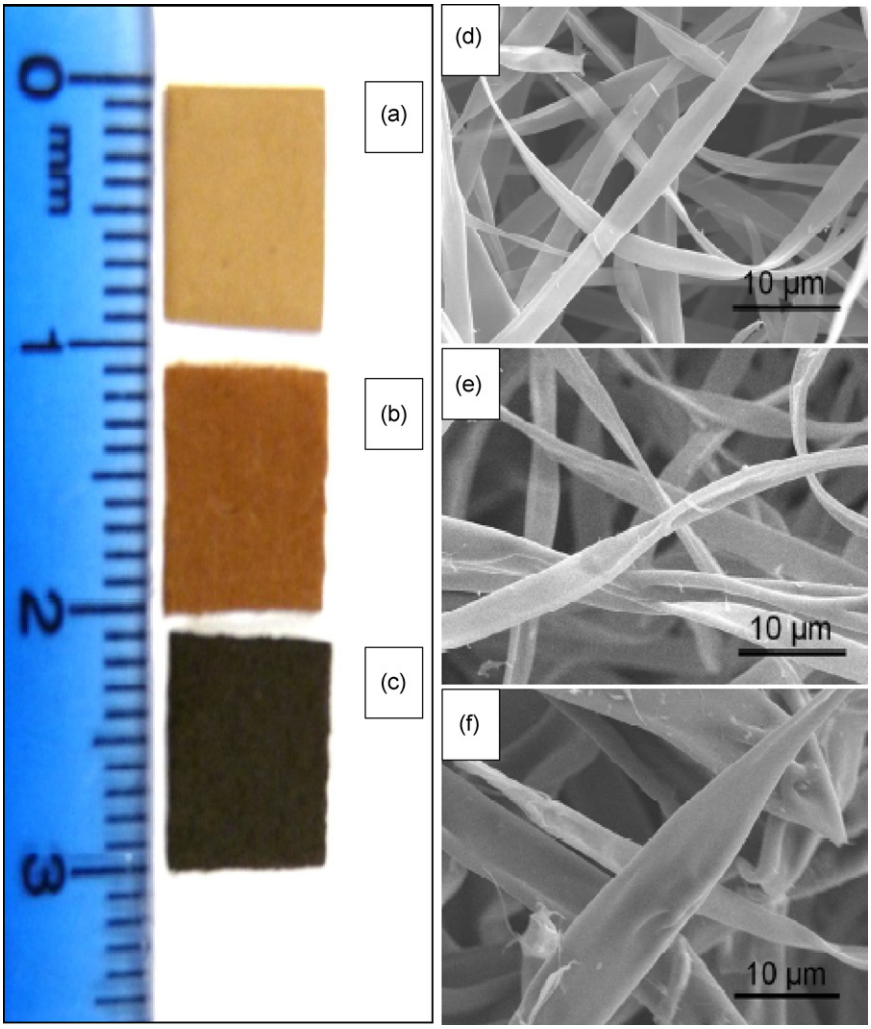

Fig. 1. Optical images (a–c) and SEM images (d–f) of the composite microbelts with the mass ratio of SWNTs to Hb of 0/175 (a and d), 5/175 (b and e), and 10/175 (c and f), respectively. The concentration of Hb in TFE is maintained at 175 mg/mL.

retains the essential features of its native secondary structure. It is also demonstrated that the electrospinning process and the use of SWNTs and TFE would not destroy the structure of Hb. As a control, SWNTs alone do not show these two typical bands for Hb. Raman was also employed to study the SWNT-Hb microbelts and the results were presented in Fig. S2B. One can see that both Raman spectra of SWNTs powder (curve a) and SWNT-Hb microbelts (curve c) show an E_{2g} graphitic peak at around 1588 cm^{-1} (G band) and an amorphous carbon peak at 1357 cm^{-1} (D band) (Cai and Chen, 2004b), while the spectrum of pure Hb microbelts (curve b) does not show these two typical G band and D band for SWNTs. These results indicate the successful incorporation of SWNTs in the composite microbelts and the high voltage of 22.5 kV applied in electrospinning process would not destroy the structure of SWNTs.

3.2. Direct electrochemistry of Hb in SWNTs–Hb microbelts

Fig. 2A shows the CVs of the bare GCE (curve a), Hb microbelts/GCE (curve b) and SWNTs–Hb microbelts/GCE (curve c) in 0.1 M pH 7.0 de-aerated phosphate buffer solution. There are no oxidation and reduction peaks observed for the bare GCE (control). On the contrary, strong redox peaks are obtained at the SWNTs–Hb microbelts/GCE, which are more prominent than those obtained at the Hb microbelts/GCE (Ding et al., 2010). The excellent performance of the SWNT-Hb microbelts can be attributed to the combination of the enhanced electron transfer by incorporated/embedded SWNTs and the porous 3-D structure of Hb microbelts. The formal potential ($E^{0'}$) calculated from the average of E_{pa} and E_{pc} is −0.281 V, which represents the characteristic of Fe(III)/Fe(II) redox couple in the heme groups and is in agreement with the reported values in the literature (He et al., 2002; Lu et al., 1997).

To further study the electron-transfer process, the effect of scan rate on the electrochemical response of the SWNTs–Hb microbelts/GCE was investigated. Fig. 2B shows the CV curves of the SWNT-Hb microbelts/GCE in 0.1 M pH 7.0 de-aerated phosphate buffer obtained at scan rates of 25, 50, 75, 100, 125, 150, 175, and 200 mV/s. It can be found that both the anodic peak current (I_{pa}) and cathodic peak current (I_{pc}) are proportional to the scan rate with correlation coefficients (R^2) of 0.999 for both I_{pa} and I_{pc}, showing a typical surface-controlled electrochemical behavior (Shan et al., 2007). Based on the CV curve, the surface coverage (Γ^*) of electroactive Hb at a GC electrode can be estimated using $Q = nFA\Gamma^*$, where Q (6.61×10^{-7} C) is the charge involved in the reaction, which can be obtained by integration of reduction peak, A is the electrode area, n (the number of electron transferred) is 1 for Fe(III)/Fe(II) redox couple, and F is the Faraday constant. Γ^* is estimated to be 9.79×10^{-11} mol/cm^2, almost 5.2 times of the theoretical value for monolayer coverage (1.89×10^{-11} mol/cm^2)

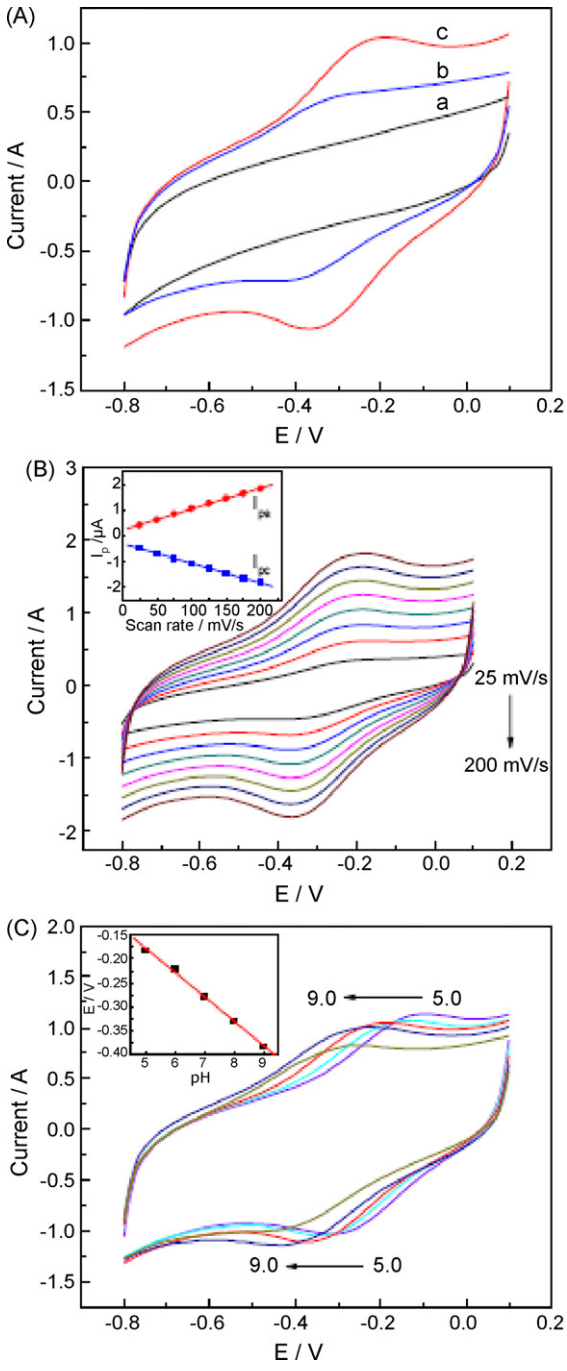

Fig. 2. (A) Cyclic voltammograms of the bare GCE (a), the Hb microbelts/GCE (b), and the SWNTs–Hb microbelts/GCE (c) in 0.1 M pH 7.0 phosphate buffer solution at a scan rate of 100 mV/s, respectively. (B) Cyclic voltammograms of the SWNTs–Hb microbelts/GCE in 0.1 M pH 7.0 phosphate buffer solution at scan rates of 25, 50, 75, 100, 125, 150, 175 and 200 mV/s. Inset: Plot of peak currents versus scan rate. (C) Cyclic voltammograms of the SWNTs–Hb/GCE in 0.1 M phosphate buffers with different pH values of 5.0, 6.0, 7.0, 8.0 and 9.0. The scan rate is 100 mV/s. Inset: The plot of the formal potential against pH.

(Wang et al., 2005). This indicates that multilayer of Hb participated in the electron-transfer process.

pH value of the electrolyte is an important parameter which can significantly affect electrochemical behavior of redox protein. The pH-dependence of the formal potential $E^{0'}$ for the redox couple indicates the participation of proton in the electrochemical process (Shan et al., 2009). As shown in Fig. 2C, nearly reversible voltammograms with stable and well-defined peaks were obtained for all of the pH values tested. An increase in electrolyte pH leads to a negative shift in peak potential. The inset of Fig. 2C shows that $E^{0'}$ is linearly proportional to the electrolyte pH with a slope of −51.1 mV/pH (R^2 = 0.996), which is close to the Nernstian value of −59.2 mV/pH at room temperature for the reversible one-electron transfer accompanied with single-proton transportation (Zhao et al., 2006). The reaction scheme for the electrochemical reduction and oxidation of Hb can be expressed as Hb hemeFe(III) + H^+ + e^- ↔ Hb hemeFe(II).

3.3. Electrocatalytic reduction and amperometric detection of H_2O_2 using the SWNTs–Hb microbelts modified GCE

CV measurements were firstly performed to investigate the electrocatalytic property of the SWNTs–Hb microbelts/GCE towards the reduction of H_2O_2. One can see from Fig. 3A, the reduction peak current obtained at the SWNTs–Hb microbelts/GCE at ca. −0.364 V was obviously increased with the increase of the concentration of H_2O_2 in the solution. As a control, the bare GCE shows insignificant reduction towards H_2O_2. Furthermore, the reduction current signal at the composite microbelts modified electrode was greatly enhanced compared to that obtained at the pristine Hb microbelts/GCE as shown in our previous work (Ding et al., 2010). These results indicate that SWNTs incorporated in Hb microbelts can significantly augment the electron transfer between Hb and the electrode and the as-prepared electrode has potential application for quantitative determination of H_2O_2 in solutions. The applicability of the SWNTs–Hb microbelts/GCE for amperometric detection of H_2O_2 was thus investigated.

Fig. 3B shows typical amperometric responses of the SWNTs–Hb/GCE to the successive addition of H_2O_2 at an applied potential of −0.364 V (the reduction peak potential for H_2O_2 at the as-prepared electrode). Upon the addition of H_2O_2, the SWNTs–Hb microbelts/GCE responded rapidly and 95% of the steady-state current could be achieved within 10 s, indicating a fast amperometric response to H_2O_2 reduction. The corresponding calibration curve is presented in Fig. 3C. It can be seen that the calibration curve is linear up to 2.73×10^{-5} M (R^2 = 0.991), with a sensitivity of 261.72 μA/mM cm^2 and a detection limit of 0.22 μM H_2O_2 (S/N = 3). The sensitivity is 7.7 times higher than that of 33.95 μA/mM cm^2 obtained for the Hb microbelts/GCE due to the enhancement of electron transfer by SWNTs. The detection limit is almost 3-fold lower than 0.61 μM of Hb microbelts/GCE without SWNTs and also better than those of recently reported Hb-based biosensors (Ding et al., 2010; Guo et al., 2008; Shan et al., 2009; Zhao et al., 2009; Zhu et al., 2007). Table S1 summarizes recently reported Hb-based amperometric H_2O_2 biosensors. It can be seen that the limit of detection of the developed biosensor is the best one among them. In addition, the calibration curve gradually reaches the plateau at high concentrations of H_2O_2, displaying a typical Michaelis–Menten kinetic behavior and gradually reaches the plateau at high concentration of H_2O_2. The apparent Michaelis–Menten constant ($K_{m,app}$) for SWNTs–Hb microbelts towards H_2O_2 reduction, which is an indicator of the affinity between the protein and substrate, can be derived from Lineweaver–Burk equation $1/I_{ss} = K_{m,app}/I_{max}C + 1/I_{max}$, where I_{ss} is the steady state current after the addition of substrate, C is the bulk concentration of the substrate, and I_{max} is the maximum current measured under the saturated substrate condition. From the Lineweaver–Burk plot (inset of Fig. 3C), the $K_{m,app}$ value is calculated to be 0.070 mM, which is smaller than 0.093 mM of Hb microbelts (Ding et al., 2010) and also significantly smaller than those of reported CNTs modified electrodes, e.g. 0.533 mM for SA-MWNTs-Hb/GC (Zhao et al., 2009), 41 mM for Nafion-Hb-CNT/GC (Cai and Chen, 2004a), and 0.928 mM for PVA-Hb-MWNTs/carbon ionic liquid electrode (Sun et al., 2009a).

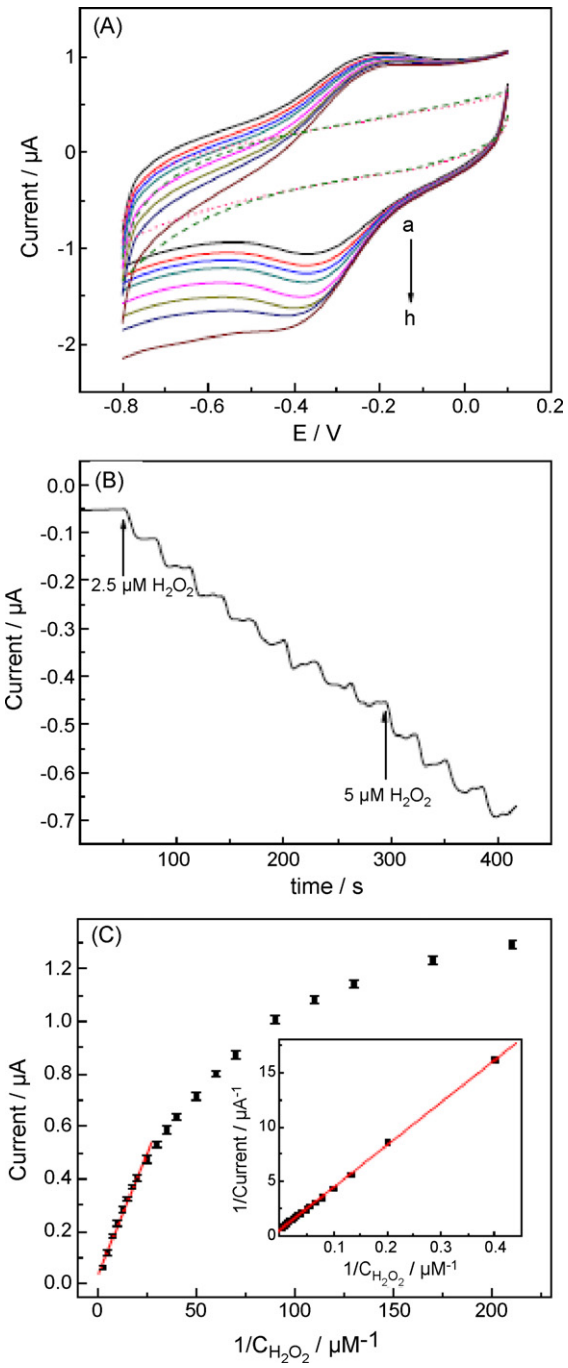

Fig. 3. (A) Cyclic voltammograms of the bare GCE (dot line: without H_2O_2, dash line: with 70 μM H_2O_2) and cyclic voltammograms of the SWNTs–Hb microbelts/GCE at a scan rate of 100 mV/s in 0.1 M pH 7.0 phosphate buffer with (a) 0, (b) 10, (c) 20, (d) 30, (e) 50, (f) 70, (g) 90, (h) 130 μM H_2O_2, respectively. (B) Amperometric response of the SWNTs–Hb microbelts/GCE with successive additions of H_2O_2 to 0.1 M pH 7.0 phosphate buffer solution at an applied potential of −0.364 V vs. Ag/AgCl. (C) The corresponding calibration plot for H_2O_2. Inset presents the Lineweaver–Burk plot.

The high sensitivity, low detection limit, and small $K_{m,app}$ value indicates that the SWNTs–Hb microbelts has excellent electrocatalytic ability towards H_2O_2 reduction as well as good biocompatibility. Such superior performance can be attributed to the enhanced direct electrochemistry by highly porous SWNTs–Hb microbelts network, ultrathin of the microbelts, and the incorporation of SWNTs. As illustrated in Scheme 1, the electrospun microbelts form a highly porous structure and possess high specific surface area, allowing the access of analytes to the active sites

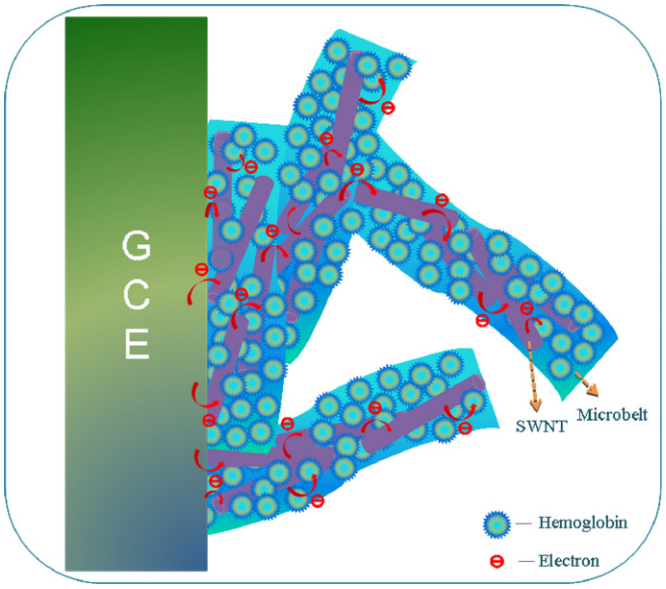

Scheme 1. Schematic illustration for the direct electron transfer from SWNTs–Hb microbelts to GCE.

of Hb with minimal diffusion resistance. Additionally, owing to their small dimensions, SWNTs are structurally compatible to Hb molecules, thus resulting in effective interaction between the redox center of Hb and SWNTs. Such interaction enables fast electron transfer between Hb and SWNTs. Furthermore, SWNTs can also provide more conducting channels to transfer electrons between Hb and the surface of electrode, thus allowing the "long-range" electron transfer. All these features attribute to the superior performance of the as-prepared SWNTs–Hb microbelts.

The reproducibility of the SWNTs–Hb microbelts modified electrode was also investigated. The electrode-to-electrode reproducibility was characterized by the low relative standard deviation (R.S.D.) of 9.35% ($n = 5$) in the response to 2.5 μM H_2O_2. The R.S.D. of 4.71% ($n = 5$) for 2.5 μM H_2O_2 using the same electrode demonstrated good intra-electrode reproducibility. In addition, there is no interference from uric acid and ascorbic acid at such low applied potential.

3.4. Electrocatalytic reduction and amperometric detection of nitrite using the SWNTs–Hb microbelts modified GCE

Nitrite can be toxic to human beings when its concentration reaches a certain level, because it can irreversibly convert hemoglobin to methemoglobin and thus cause hemoglobin losing oxygen uptake and transport capability. Based on the regulation of U.S. EPA, the maximum contaminant level (MCL) for nitrite ion in drinking water is 1 ppm (21.7 μM) (Daniel et al., 2009). As nitrite is widely presented in environment, beverages and food products, there is an urgent need to develop sensitive and selective biosensor for its quantitative determination. The applicability of the SWNT-Hb modified GCE for nitrite detection was further investigated. Compared to the CV of the SWNTs–Hb microbelts/GCE in 0.05 mM pH 4.0 BR buffer, the addition of nitrite results in a new reduction peak at ca. −0.65 V and the peak current increased with the nitrite concentration (Fig. 4A). The reduction peak may stem from [Hb Fe(II)$(NO)^+$]$^+$ following the possible reaction routes described elsewhere (Mimica et al., 2001; Yang et al., 2005). By contrast, the reduction of nitrite at bare GCE is not obvious.

The peak potential of −0.65 V was then used as the working potential for amperometric detection of nitrite. As shown in Fig. 4B,

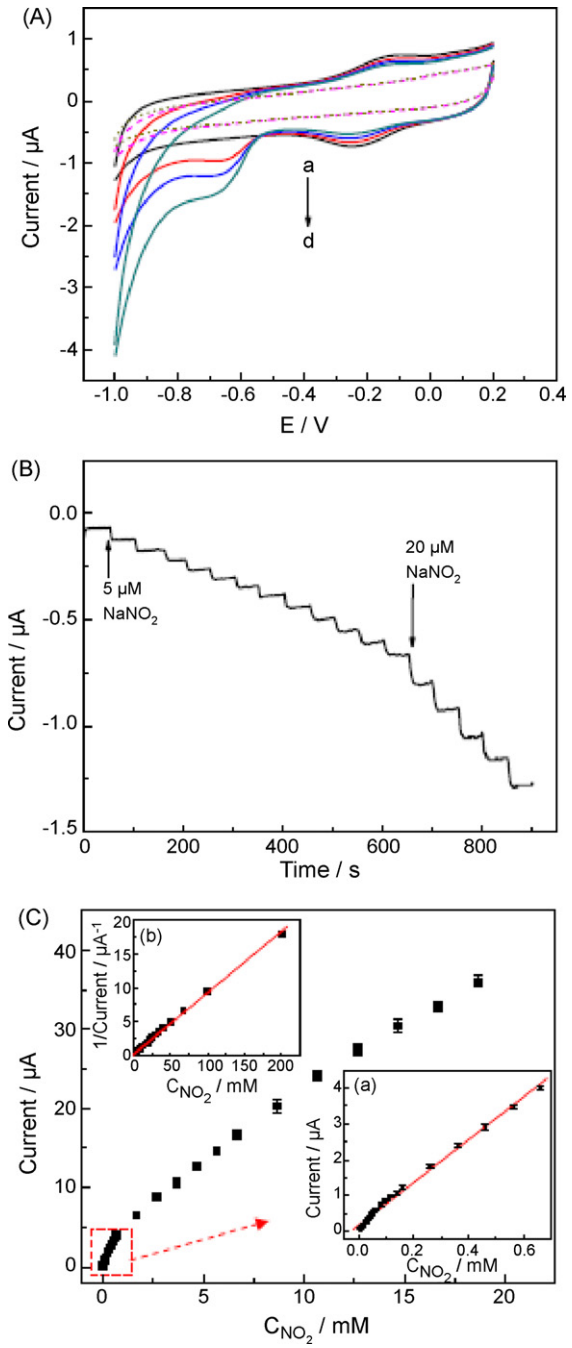

Fig. 4. (A) Cyclic voltammograms of the bare GCE (dot line: without $NaNO_2$, dash line: with 200 μM $NaNO_2$) and the SWNTs–Hb microbelts/GCE at a scan rate of 100 mV/s in 0.1 M pH 4.0 BR buffer with (a) 0, (b) 200, (c) 400 and (d) 800 μM $NaNO_2$, respectively. (B) Amperometric response of the SWNTs–Hb microbelts/GCE with successive additions of $NaNO_2$ to 0.1 M pH 4.0 BR buffer solution at an applied potential of −0.65 V vs. Ag/AgCl. (C) The corresponding calibration plot for $NaNO_2$. Insets: Enlarged drawing of calibration plot in the range of low $NaNO_2$ concentrations (a) and the Lineweaver–Burk plot (b).

the amperometric response towards nitrite reduction showed a linear relationship up to 2.07×10^{-4} M ($R^2 = 0.994$) (Fig. 4C, inset a), with a sensitivity of 84.84 μA/mM cm^2 and a detection limit of 0.30 μM (S/N = 3). Compared with pure Hb microbelts modified electrode, both the sensitivity and detection limit of the SWNTs–Hb/GCE are better (Ding et al., 2010). In addition, the detection limit is remarkably better than other reported values in the literature (Dai et al., 2004; Yu et al., 2007) and can also satisfy the requirement for the detection of EPA MCL nitrite (21.7 μM). Table S2 summarizes different Hb-based nitrite sensors. One can clearly see the improvement in the performance for SWNTs–Hb microbelts based biosensor. From the Lineweaver–Burk plot (Fig. 4C, inset b), the $K_{m,app}$ value of the developed nitrite biosensor was calculated to be 0.49 mM, which is better than 0.71 mM for pure Hb microbelts (Ding et al., 2010) and also more than 10 times smaller than 7.48 mM for Hb in titania sol–gel film (Zhao et al., 2006) and 9.4 mM for Hb entrapped in PVA-ionic liquid (Zhang et al., 2009). These results once again demonstrate the critical role of SWNTs incorporated into the composite microbelts and also indicate that the SWNTs–Hb microbelts based biosensor is an ideal analytical tool for sensitive detection of nitrite in solutions.

The reproducibility of the proposed sensor towards nitrite detection was also studied. The R.S.D. of inter-electrode responses to 20 μM nitrite at five different electrodes was 7.64% while the R.S.D of intra-electrode responses to five-time repeated additions of 20 μM nitrite was 3.89%. Furthermore, the interference study shows that 4 mM KNO_3, $MgCl_2$, NaI, Na_2CO_3, and NaCl do not interfere with the detection of 20 μM nitrite.

3.5. Electrocatalytic reduction and amperometric detection of TCA using the SWNTs–Hb microbelts modified GCE

TCA is another toxic compound in environment. In the United States, the maximum contaminant level goal (MCLG) for TCA in drinking water is 0.3 mg/L (1.84 μM). Thus, it is necessary to develop a biosensor for fast and sensitive detection of TCA. To explore the applicability of the SWNTs–Hb microbelts/GCE for TCA biosensing, CVs were carried out to demonstrate the electrochemical reduction of TCA at the as-prepared electrode. As shown in Fig. 5A, the electrochemical reduction of TCA at the SWNTs–Hb microbelts/GCE starts at ca. −0.4 V and the reduction current increases sharply with the potential towards the negative end, while the reduction signal of TCA at the bare GCE is insignificant. As a demonstration towards sensitive amperometric detection of TCA, an applied potential of −0.65 V was used and the amperometric detection was carried out in 0.1 M pH 7 phosphate buffer (Fig. 5B). The linear range of the amperometric response was obtained from 1.2×10^{-5} to 1.08×10^{-4} M, with a sensitivity of 28.577 μA/mM cm^2 and a detection limit of 2.41 μM (S/N = 3) (Fig. 5C). As shown in Table S3, the detection limit is 3-order magnitude lower than previous reports, e.g. 10 mM for Nafion-SWNTs–Hb/CILE (Sun et al., 2008) and 8.5 mM for Nafion-nano ZnO-Hb/CILE (Sun et al., 2009b). This detection limit is slightly higher than the U.S. maximum contaminant level goal for TCA (1.84 μM). However, the detection limit, which is obtained not under optimum conditions, can be greatly improved by optimizing the operating conditions such as buffer pH and the applied potential (more negative applied potentials, e.g. −0.8 V, favor TCA reduction), thus satisfying the sensitivity requirement for environmental monitoring of TCA. The $K_{m,app}$ derived from the Lineweaver–Burk plot (Fig. 5C, inset) was 0.24 mM, which is also significantly lower than other reported values (Sun et al., 2007; Yang et al., 2008), indicating the good biocompatibility of SWNTs–Hb microbelts.

The reproducibility for TCA detection was also excellent, demonstrated by low R.S.D. values of inter-electrode responses to 80 μM TCA (8.39%, five different electrodes) and intra-electrode responses to five-time repeated additions of 80 μM TCA (7.54%).

3.6. Stability and spiked real sample test

The stability of SWNTs–Hb microbelts/GCE was examined by CV. As shown in Fig. S3, the CVs obtained at different storing time show minor changes for 1 week. In addition, the amperometric responses in 2 weeks only show 10.4%, 4.8% and 8.3% decrease in the current responses to 2.5 μM H_2O_2, 20 μM nitrite and 100 μM TCA, respec-

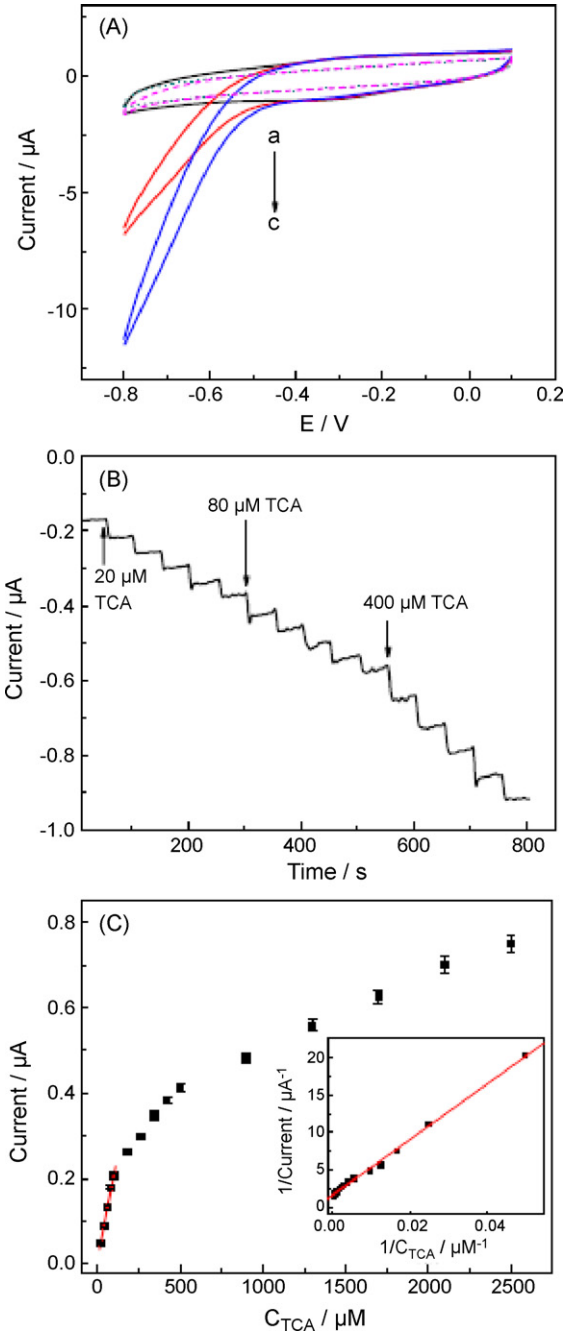

Fig. 5. (A) Cyclic voltammograms of the bare GCE (dot line: without TCA, dash line: with 5 mM TCA) and the SWNTs–Hb microbelts/GCE at a scan rate of 100 mV/s in 0.1 M pH 7.0 phosphate buffer with (a) 0, (b) 5, (c) 7 mM TCA, respectively. (B) Amperometric response of the SWNTs–Hb microbelts/GCE with successive additions of TCA to 0.1 M pH 7.0 phosphate buffer solution at an applied potential of −0.65 V vs. Ag/AgCl. (C) The corresponding calibration plot of amperometric response towards TCA. Inset presents the Lineweaver–Burk plot.

tively. The good stability may be attributed to tight attachment of the microbelts film on the surface of electrode and no leakage of SWNTs or Hb from the microbelts.

Real sample tests were conducted using spiked tap water. The detection of the spiked tap water was calibrated by the response to the analytes in buffer solution. The amperometric responses were shown in Fig. S4. One can see that there is almost no difference between the responses to the analytes in the buffer and in the tap water, indicating the potential practical application of our proposed sensor for H_2O_2, nitrite or TCA in real samples.

4. Conclusions

SWNTs–Hb microbelts were directly electrospun onto the GCE to fabricate novel composite microbelts based biosensor for sensitive and mediator-free detection of H_2O_2, nitrite, and TCA. Raman spectra indicated that SWNTs were successfully incorporated into the microbelts and still possessed the characteristic G band and D band. FT-IR spectra were performed to demonstrate that the electrospinning process and the incorporation of SWNTs into Hb microbelts would not destroy the native structure of Hb. The effect of scan rate and electrolyte pH on the direct electrochemistry of the as-prepared electrode was investigated. A comparative study of three-electrodes (bare GCE, Hb microbelts/GCE, and SWNTs–Hb microbelts/GCE) demonstrates that the incorporation of SWNTs into Hb microbelts can significantly enhance the direct electron transfer between Hb and electrode, and thus improve the electrocatalytic capability towards H_2O_2, nitrite, and TCA reduction. Sensitive amperometric detection of these analytes is also demonstrated. In addition, the calculated apparent Michaelis–Menten constants for H_2O_2, nitrite, and TCA are significant better than other values reported in the literature. This work is the first study on incorporating SWNTs into electrospun protein microbelts and the results show that this type of composite microbelts is an ideal material in the construction of sensitive and mediator-free biosensors.

Acknowledgements

We greatly appreciate the funding from NSF and USGS. YD also acknowledges the support from the UConn CESE through the Graduate Student Research Assistantship Program in Support of Multidisciplinary Environmental Activities by Faculty Members.

Appendix A. Supplementary data

Supplementary data associated with this article can be found, in the online version, at doi:10.1016/j.bios.2010.07.124.

References

Cai, C.X., Chen, J., 2004a. Anal. Biochem. 325, 285–292.
Cai, C.X., Chen, J., 2004b. Anal. Biochem. 332, 75–83.
Cai, W.Y., Feng, L.D., Liu, S.H., Zhu, J.J., 2008. Adv. Funct. Mater. 18, 3127–3136.
Chen, S.H., Ynan, R., Chai, Y.Q., Yin, B., Xu, Y., 2008. Electroanalysis 20, 2141–2147.
Dai, Z., Liu, S., Ju, H., Chen, H., 2004. Biosens. Bioelectron. 19, 861–867.
Daniel, W.L., Han, M.S., Lee, J.S., Mirkin, C.A., 2009. J. Am. Chem. Soc. 131, 6362–6363.
Ding, Y., Wang, Y., Li, B., Lei, Y., 2010. Biosens. Bioelectron. 25, 2009–2015.
Gao, R., Shangguan, X., Qiao, G., Zheng, J., 2008. Electroanalysis 20, 2537–2542.
Guo, C., Hu, F., Li, C.M., Shen, P.K., 2008. Biosens. Bioelectron. 24, 819–824.
Han, X., Huang, W., Jia, J., Dong, S., Wang, E., 2002. Biosens. Bioelectron. 17, 741–746.
He, P.L., Hu, N.F., Zhou, G., 2002. Biomacromolecules 3, 139–146.
He, X.Y., Zhu, L., 2006. Electrochem. Commun. 8, 615–620.
Kapoor, S., Mandal, S.S., Bhattacharyya, A.J., 2009. J. Phys. Chem. B 113, 14189–14195.
Liu, Y., Liu, H.Y., Hu, N.F., 2005. Biophys. Chem. 117, 27–37.
Lu, Z., Huang, Q., Rusling, J.F., 1997. J. Electroanal. Chem. 423, 59–66.
Maduralveeran, G., Ramaraj, R., 2007. J. Electroanal. Chem. 608, 52–58.
Mimica, D., Zagal, J.H., Bedioui, F., 2001. J. Electroanal. Chem. 497, 106–113.
Njagi, J., Chernov, M.M., Leiter, J.C., Andreescu, S., 2010. Anal. Chem. 82, 989–996.
Shan, D., Cheng, G.X., Zhu, D.B., Xue, H.G., Cosnier, S., Ding, S.N.A., 2009. Sens. Actuators B: Chem. 137, 259–265.
Shan, D., Wang, S.X., Xue, H.G., Cosnier, S., 2007. Electrochem. Commun. 9, 529–534.
Suedee, R., Intakong, W., Lieberzeit, P.A., Wanichapichart, P., Chooto, P., Dickert, F.L., 2007. J. Appl. Polym. Sci. 106, 3861–3871.
Sun, W., Gao, R.F., Jiao, K., 2007. J. Phys. Chem. B 111, 4560–4567.
Sun, W., Li, X., Zhai, Z., Jiao, K., 2008. Electroanalysis 20, 2649–2654.
Sun, W., Li, X.Q., Wang, Y., Zhao, R.J., Jiao, K., 2009a. Electrochim. Acta 54, 4141–4148.
Sun, W., Zhai, Z.Q., Wang, D.D., Liu, S.F., Jiao, K., 2009b. Bioelectrochemistry 74, 295–300.
Wang, S.F., Chen, T., Zhang, Z.L., Shen, X.C., Lu, Z.X., Pang, D.W., Wong, K.Y., 2005. Langmuir 21, 9260–9266.
Yang, J., Pang, F.Y., Zhang, R.Y., Xu, Y., He, P.A., Fang, Y.Z., 2008. Electroanalysis 20, 2134–2140.

Yang, W.W., Bai, Y., Li, Y.C., Sun, C.Q., 2005. Anal. Bioanal. Chem. 382, 44–50.
Yu, J.J., Ma, J.R., Zhao, F.Q., Zeng, B.Z., 2007. Electrochim. Acta 53, 1995–2001.
Zhang, Y.F., Yan, R., Zhao, F.Q., Zeng, B.Z., 2009. Colloid Surf. B: Biointerfaces 71, 288–292.
Zhao, H.Y., Zheng, W., Meng, Z.X., Zhou, H.M., Xu, X.X., Li, Z., Zheng, Y.F., 2009. Biosens. Bioelectron. 24, 2352–2357.
Zhao, S., Zhang, K., Sun, Y.Y., Sun, C.Q., 2006. Bioelectrochemistry 69, 10–15.
Zhu, J.T., Shi, C.G., Xu, J.J., Chen, H.Y., 2007. Bioelectrochemistry 71, 243–248.